Spatial Downscaling of Monthly TRMM Precipitation Based on EVI and Other Geospatial Variables Over the Tibetan Plateau From 2001 to 2012

Authors: Shi, Yuli, and Song, Lei

Spatial Downscaling of Monthly TRMM Precipitation Based on EVI and Other Geospatial Variables Over the Tibetan Plateau From 2001 to 2012

Yuli Shi[1,2]* and Lei Song[1]

*Corresponding author: ylshi.nuist@gmail.com

[1] *Nanjing University of Information Science and Technology, Nanjing 210044, China*

[2] *State Key Laboratory of Remote Sensing Science, Jointly Sponsored by the Institute of Remote Sensing and Digital Earth of China Academy of Sciences and Beijing Normal University, Beijing 100101, China*

Recent developments in hydrological modeling and biomass retrieval in complex mountain areas have heightened the need for accurate precipitation data at high spatial resolution. The Tropical Rainfall Measuring Mission (TRMM) provides rainfall estimates for certain climate models in mountain ranges where rain gauges are lacking. TRMM precipitation estimates, however, inherently have large uncertainties because of their coarse spatial resolution. In this study, we investigate a statistical downscaling calibration procedure to derive high-spatial-resolution (1-km) precipitation maps for the Tibetan Plateau using the satellite-based data set Enhanced Vegetation Index (EVI) from the Moderate Resolution Imaging Spectroradiometer, a digital elevation model from the Shuttle Radar Topography Mission, and the TRMM 3B43 product. Spatial downscaling from 0.25° to 1 km was achieved by using the nonparametric statistic relationships between precipitation and EVI, altitude, slope, aspect, latitude, and longitude. An additive method was used to calibrate the downscaled precipitation data. The best 1-km resolution annual precipitation data for 2001–2012 over the Tibetan Plateau were generated through downscaling and additive calibration for most cases. The results show that the method improves the accuracy of rainfall estimates. Monthly 1-km precipitation data were also obtained by disaggregating 1-km annual downscaled estimates with monthly fractions of annual total precipitation. Monthly precipitation predictions are in good agreement with rain gauge data. The calibration of the monthly product with rain gauge data significantly reduced the bias value. Overall we conclude that the methodology is useful for areas with varied climate conditions and complex topography. These results have practical implications for calculating hydrological balances, mapping aboveground biomass, and assessing regional climate change.

Introduction

Precipitation is one of the most dynamic components of the water cycle and plays a key role in matter and energy exchange in Earth's water, atmosphere, and soil cycles. The amount of precipitation influences soil moisture, vegetation growth, and stream flow (Goovaerts 2000; Guo et al 2004; Schuurmans and Bierkens 2007; Michaelides et al 2009; Langella et al 2010). But data in mountain regions are often difficult to collect, especially in such remote regions as the Tibetan Plateau, requiring downscaling of satellite-based precipitation data to generate high-resolution estimates with geospatial factors to assess regional climate change and manage water resources for regions with varied climatic conditions and complex topography.

The continuing development of reliable, spatially explicit ecological and hydrological models has led to increasing interest in methods for obtaining accurate precipitation data sets at high spatial and temporal resolution (Kyriakidis et al 2001; Giannoni et al 2003). Conventional ground measurements and remote sensing estimation are 2 ways to accomplish this task. Spatial interpolation of precipitation data from irregularly spaced weather stations is frequently used to obtain spatially continuous data. However, more interpolation errors occur in areas where gauges are sparsely distributed. Satellite-based measurement methods are

designed to address this limitation and can be used to generate precipitation data over a large area when combined with rain gauge data. A range of regional and global precipitation products exists, including rain gauge stations, satellites, and other observations, such as the Global Precipitation Climatology Project, Global Satellite Mapping of Precipitation Project, and Tropical Rainfall Measuring Mission (TRMM), which has been offering several rainfall products since 1997 with the first space-borne precipitation radar (Huffman et al 1997; Kubota et al 2007). A problem with satellite-based rainfall data products is their generally coarse resolution; the TRMM 3B43 data set has one of the highest resolutions (0.25 × 0.25°) currently available.

Several studies have focused on statistical downscaling of TRMM products to obtain high-resolution rainfall data (Immerzeel et al 2009; Quiroz et al 2011; Duan and Bastiaanssen 2013; Hunink et al 2014). The methods are generally based on the relationship between precipitation and geospatial variables (eg vegetation indexes, including the Normalized Difference Vegetation Index [NDVI]) built at coarse spatial resolution, and generate annual regional precipitation data at 1-km resolution. Schemes for statistical spatial downscaling of precipitation products vary in 3 ways: (1) the model used to predict the precipitation at fine resolution, (2) the geospatial predictors in the regression model, and (3) calibration of the downscaled rainfall products.

Several attempts have been made to build linear and nonlinear models at coarse resolution. Agam et al (2007) developed linear, polynomial, and exponent models for spatial sharpening of imagery. Immerzeel et al (2009) proposed an NDVI-based exponential statistical regression model, which was used to downscale precipitation data for the Iberian Peninsula from the TRMM monthly product. Jia et al (2011) developed a statistical linear regression model by introducing the NDVI and elevation of the Qaidam Basin in China. Duan and Bastiaanssen (2013) and Hunink et al (2014) also applied parameterized regression using geospatial data to improve TRMM rainfall estimates in mountainous areas. The latter 2 studies improved the spatial resolution of the TRMM annual, monthly, and weekly precipitation data from 0.25° (approximately 28 km) to 1 km. Based on Immerzeel's method, Park (2013) decomposed TRMM precipitation data into trend and residual components and used a geostatistical regression model to downscale the data to 1-km resolution. Considering the spatial variation of precipitation, Chen et al (2014) also disaggregated the TRMM monthly precipitation data according to a geographically weighted regression model. Zheng and Zhu (2014) presented a hybrid regression model with residual correction for downscaling annual TRMM 3B43 data for northern China from 2000 to 2009 from 0.25° to 1-km grids. Heidinger et al (2012) applied multiresolution analysis to improve TRMM 3B42 daily

rainfall estimates at 19 meteorological stations on the Andean Plateau. And Quiroz et al (2011) used a wavelet transform to improve daily rainfall estimation from NDVI.

These models are site based and perform well at a small regional scale. Compared with linear and nonlinear regression, our initial research found that nonparametric regression models constructed using the random forests (RF) algorithm can potentially improve the performance of precipitation predictions for large areas (Xia 2014). RF is a nonparametric statistical regression algorithm that combines tree predictors depending on the values of a random vector sampled independently. Each tree of the RF has the same distribution in the forest (Breiman 2001; Liaw and Wiener 2002). RF has been shown to be an effective and robust algorithm and has been applied in ecological, climatic, and many other fields (Chan and Paelinckx 2008; Wei et al 2010; Ibarra-Berastegi et al 2011; Stumpf and Kerle 2011; Vincenzi et al 2011; Yu et al 2011). In this study, we concentrated on developing the current downscaling methodology further and estimated precipitation with a machine-learning algorithm used in the model construction process.

NDVI is one of the key predictors used in downscaling methods. Many studies have found a positive correlation between NDVI and precipitation (Immerzeel et al 2009; Jia et al 2011; Duan and Bastiaanssen 2013; Hunink et al 2014). As vegetation's sensitivity to precipitation is cumulative rather than instantaneous (Gessner et al 2013), NDVI daily and monthly data on responses to precipitation have a time lag (Immerzeel et al 2005). The time lag can be up to 1–3 months (Quiroz et al 2011), which means that NDVI-based downscaling is applicable only at annual time scales (Duan and Bastiaanssen 2013). NDVI-based downscaling methods may also be problematic when precipitation is over a certain value in humid areas. Therefore, it is necessary to find another vegetation index to replace the NVDI for downscaling of precipitation data. The Enhanced Vegetation Index (EVI) was developed to optimize the vegetation signal with improved sensitivity in high-biomass regions and to improve vegetation monitoring through a decoupling of the canopy background signal. Several investigations have indicated that EVI potentially improves the relatively weak empirical relationships between precipitation and the saturated NDVI in humid areas (Justice et al 1998; Huete et al 2002). EVI thus might be a better predictor of precipitation. Further key elements for downscaling include elevation, aspect, and slope, extracted from a digital elevation model (DEM). A clear relationship between elevation and precipitation has been reported in previous studies, and Jia et al (2011) improved downscaling results after inclusion of elevation data. Park (2013) also employed a DEM, a vegetation index, and a downscaling scheme to produce downscaling results that

reflected detailed characteristics with better predictive performance.

Another problem that influences the accuracy of final precipitation data is the difference between downscaled precipitation data and the measurements from rain gauge stations. Reliable and robust calibration methods can minimize the gaps and greatly improve the accuracy of downscaled precipitation data. Hughes and Smakhtin (1996) used geographical differential analysis (GDA) to patch and extend observed time series of daily stream flow. Cheema and Bastiaanssen (2012) used GDA to calibrate TRMM rainfall data for the Indus River basin. Duan and Bastiaanssen (2013) evaluated the GDA method in an attempt to obtain disaggregated 1-km monthly precipitation data for the humid Lake Tana basin of Ethiopia. In this study, we extended GDA to correct the bias of the downscaled precipitation data using rainfall data from 91 rain gauge stations on the Tibetan Plateau.

This study had 3 steps. First, we developed a downscaling method involving a machine learning algorithm to estimate annual precipitation with 6 predictors including EVI, elevation, slope, aspect, latitude, and longitude. The regression models used to estimate precipitation were trained and evaluated at coarse resolution over a variety of arid to humid regions in the Tibetan Plateau. Second, we generated maps of annual precipitation on the Tibetan Plateau at 1-km spatial resolution by applying the downscaling procedure to original annual TRMM 3B43 data for 2001 to 2012, and then produced maps of monthly precipitation by disaggregating annual data using a simple fraction method. Third, we investigated a calibration method involving simple kriging, using rain gauge data, to see whether it could improve the accuracy of annual and monthly precipitation estimates. The ground measurements include 12 years (2001–2012) of monthly precipitation data collected at 91 rain gauge stations across the Tibetan Plateau.

This study has practical implications for hydrologists and climate researchers who need to calculate hydrological balances, map aboveground biomass, and assess regional climate change, and require precipitation estimates at finer resolution for use in hydrological and climate models for regions with complex terrain and sparse networks for rainfall measurement.

Study area

This study focuses on the Tibetan Plateau, an area of about 2.57 million km^2 (Zhang et al 2002) located in eastern Asia ranging from $26°00'12''$ to $39°46'50''$N and $73°18'52''$ to $104°46'59''$E (Figure 1A). The mean elevation of the Tibetan Plateau is above 4000 m. It is the highest plateau in the world and is often called the roof of the

world. Its special topography and location lead to complex climatic conditions and varied vegetation (Zhisheng et al 2001).

Under the influence of the Asian monsoon and westerlies, there is a clear demarcation between the dry and the rainy seasons; about 90% of the precipitation occurs in the rainy season. The average air temperature ranges from 7 to 15°C in the warmest month (July) to −1 to −7°C in the coldest month (January) (Zhong et al 2011). The east Asian monsoon prevails in the eastern part of the Tibetan Plateau but brings less precipitation because the Hengduan Mountains block most of the moist air from the sea from entering this area (Shen et al 2011). The central and southern part of the plateau, influenced by the Indian monsoon, sees more precipitation. The western and northern part of the plateau is arid because no monsoon reaches it. During the last decade, most precipitation in the eastern and northern Tibetan Plateau has fallen in June, July, and August (JJA) and March, April, and May, and there has been almost no precipitation in December, January, and February (DJF); most precipitation in the southern and central parts of the plateau occurs in JJA and almost no precipitation in other seasons; most precipitation in the western plateau (except for the Karakoram and Pamir regions) falls in JJA and a little in DJF (Maussion et al 2014).

The vegetation of the Tibetan Plateau consists of grasslands, forest, and shrublands (Shen et al 2011). Grass, including meadows and steppe, occupies about 70% of the plateau, mostly in the central part (Piao et al 2011) (Figure 1B). Most vegetation is deciduous (Ran et al 2009). The growing season is from April to October, with a growth peak during July and August, which is consistent with the precipitation pattern (Che et al 2014). Therefore, a strong positive correlation between precipitation and vegetation cover can be observed (at an annual, not monthly, scale), which serves as the foundation for the algorithm for downscaling spatial precipitation (Almazroui 2011).

Data sets and processing

Enhanced Vegetation Index

The EVI maintains sensitivity in dense vegetation conditions while minimizing canopy background variations. For this reason, we assume that the correlation between EVI and rainfall is closer than that between the NDVI and rainfall, particularly in humid regions. The Moderate Resolution Imaging Spectroradiometer EVI product, MOD13A3, was used in this study and preprocessed for geometric, radiometric, and atmospheric correction. MOD13A3 data are a gridded level-3 product at 1-km spatial resolution. When generating this monthly product, the algorithm

FIGURE 1 Tibetan Plateau. (A) Location and elevation of the plateau and location of 91 meteorological stations used for calibration and validation; (B) vegetation map. (Map A by station information of China ground climate data set and DEM from the Shuttle Radar Topography Mission; map B by Moderate Resolution Imaging Spectroradiometer global land cover product MCD12Q1)
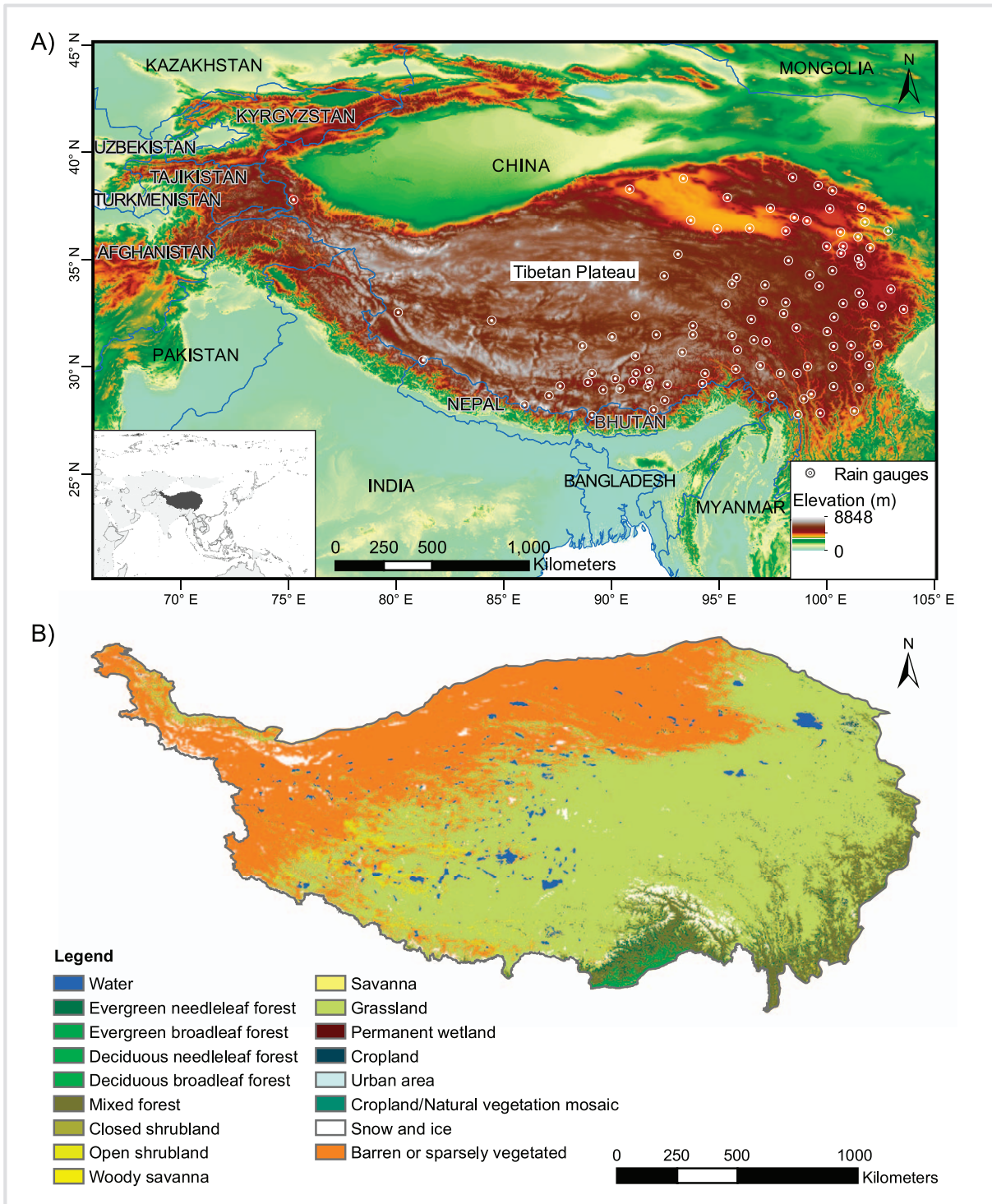
incorporates all 16-day 1-km products that overlap during the month and employs a weighted temporal average if data are cloud free, or a maximum value in case of clouds. This 1-km monthly data set was obtained from the Land Processes Distributed Active Archive Center (https://lpdaac.usgs.gov/products/modis_products_table/mod13a3). We aggregated the MOD13A3 data into the annual EVI for the Tibetan Plateau for 2001–2012 at a spatial resolution of 1 km. In the aggregated EVI product, each pixel contained the average maximum monthly value of the EVI.

Tropical Rainfall Measuring Mission

In order to measure tropical and subtropical rainfall, the TRMM Multisatellite Precipitation Analysis provides a calibration-based sequential scheme for combining precipitation estimates from multiple satellites and gauge analyses since 1998 (Kummerow et al 2000). The TRMM Version 7 3B43 data set used in this study is one of several TRMM precipitation products at different time scales. The data set covers the latitude band 50°N–S for 1998 to the present at a resolution of $0.25 \times 0.25°$ (Huffman et al 2007; Jia et al 2011). The Global Precipitation Climatology Center gauge analysis has been integrated in the land values of TRMM Version 7 3B43 (Huffman and Bolvin 2013), which seemingly corrected the land bias in most places by construction. We aggregated TRMM 3B43 monthly precipitation data for the Tibetan Plateau into annual total precipitation for 2001 to 2012. The TRMM 3B43 data set used in this study was obtained from the International Scientific and Technical Data Mirror Site for the Computer Network Information Center of the Chinese Academy of Sciences (http://www.gscloud.cn/).

Shuttle Radar Topography Mission DEM

We used a DEM from the Shuttle Radar Topography Mission to analyze the influence of topography on precipitation. This DEM, with a spatial resolution of 3 arc seconds (roughly 90 m), covers land surface between latitudes 60°N and 56°S, which includes approximately 80% of the earth's surface. We downloaded the DEM data from the website of the CGIAR Consortium for Spatial Information (http://srtm.csi.cgiar.org/SELECTION/inputCoord.asp) and extracted elevation, slope, and aspect data from it using ArcGIS. All data were resampled to 1-km resolution using pixel averaging, to match the EVI data.

Rain gauge data

Annual and monthly precipitation data for 2001–2012 were downloaded from the website (http://www.escience.gov.cn/metdata/page/index.html). These data were gathered from 91 rain gauges at national weather stations on the Tibetan Plateau, where precipitation was measured with unheated tipping buckets or traditional Hellman gauges, and the resulting data underwent rigorous quality control. We randomly split monthly rain gauge data into 2 sample sets. The first set was used to calibrate the monthly disaggregated precipitation data using the additive calibration method, and the second set was used to provide independent validation sets to test the stability of this method. The locations of national weather stations on the Tibetan Plateau are shown in Figure 1A.

Methodology

The statistical analysis conducted in this study consisted of 4 main steps: training (modeling), downscaling, calibrating, and disaggregating. First, a nonparametric regression model was established and evaluated using the RF algorithm at coarse resolution. Next, the regression model was employed to predict precipitation at fine spatial scale, and the downscaled results were obtained by adding the residual terms. The downscaled data were then calibrated using GDA and disaggregated to generate monthly precipitation data. These steps are illustrated in Figure 2 and described in more detail below.

The RF model

RF is an ensemble learning technique for classification and regression tasks that consists of a collection of N trees $\{\Theta_1(X), \Theta_2(X), ..., \Theta_N(X)\}$, where $\{X = x_1, x_2, ..., x_p\}$ is a p-dimension input vector. For an input vector X, N outputs were generated according to each tree, $Y_1 = \Theta_1(X), ..., Y_N = \Theta_N(X)$, where Y_n is the nth tree output variable, n = 1, ..., N. The final outcome is the average of the results of all the trees (Breiman 2001; Liaw and Wiener 2002).

Three parameters need to be determined in the process of building the model: *ntree*, the number of regression trees grown corresponding to a bootstrap sample of the observations; *mtry*, the number of different predictors tested at each node of a tree; and *nodesize*, the minimal size of the terminal nodes of the trees. The RF regression algorithm performs as follows (Liaw and Wiener 2002):

- Randomly draw *ntree* bootstrap samples x_i (i = bootstrap iteration) with replacement from the training data set. The elements not included in X_i are referred to as out-of-bag (OOB) data for that bootstrap sample.
- For each bootstrap sample, grow an unpruned regression tree with the modification that at each node, randomly sample *mtry* of the predictors, and choose the best split from among those variables.
- Predict new data (OOB elements) by averaging predictions of the *ntree* trees.
- The OOB samples in the training data were used to estimate prediction error, in which the OOB samples

FIGURE 2   Workflow for statistical downscaling and calibration of TRMM 3B43 annual precipitation data.
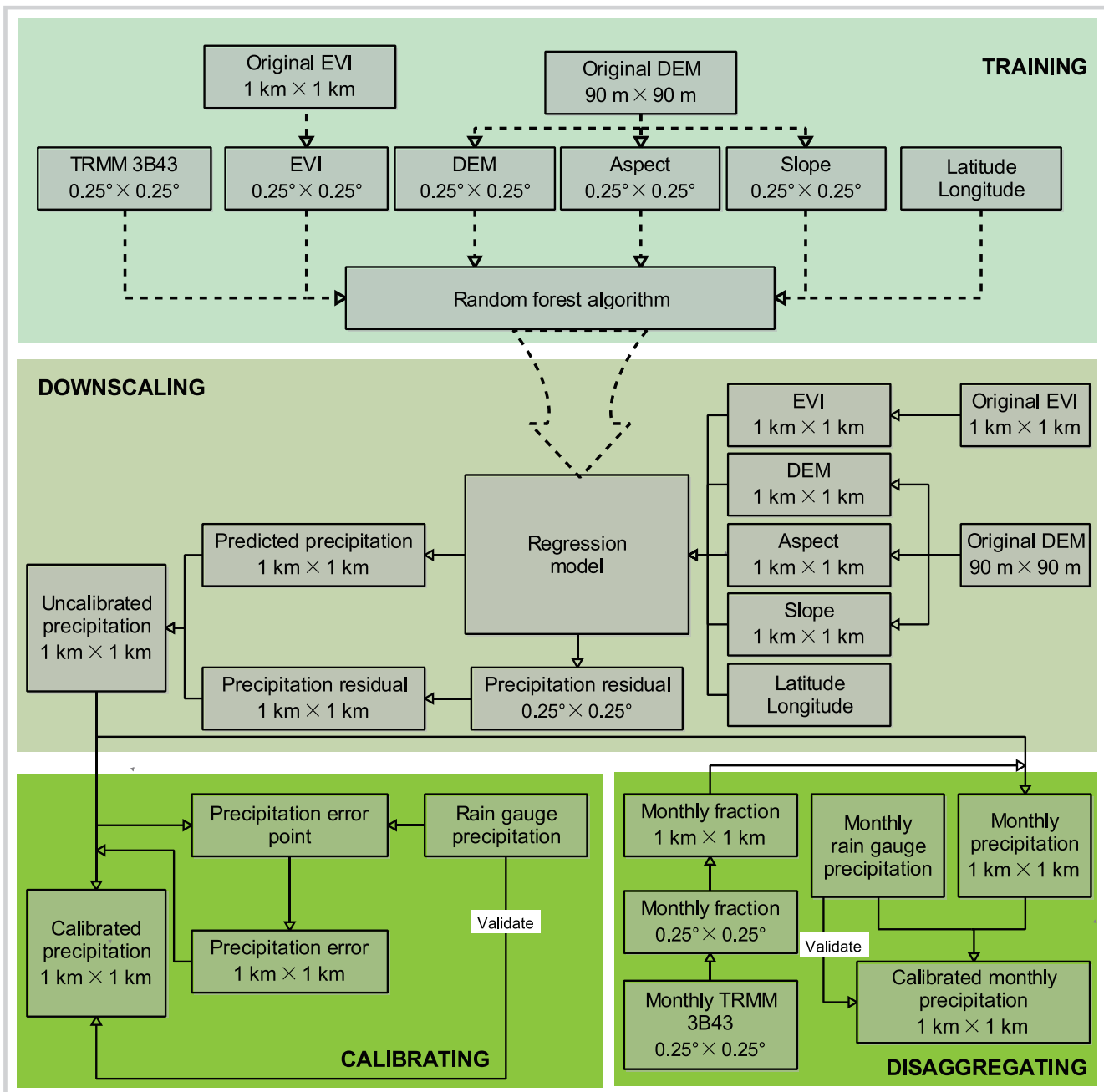
were predicted by the respective trees and by aggregating the predictions. The OOB estimate of the error rate was calculated as follows (Cutler et al 2012):

$$\text{MSE}_{oob} = \frac{1}{N}\sum_{i=1}^{N}\left(y_i - \hat{f}_{oob}[\text{X}_i]\right)^2 \qquad (1)$$

where $\hat{f}_{oob\text{-}}(\text{x}_i)$ is the OOB prediction observation i.

The RF algorithm can also generate a measure of variable importance by looking at how much prediction error increases when OOB data for that specific predictor variable are permuted while the values of other predictors are kept unchanged. These variable importance values are then used to rank the predictors in terms of their relative contribution to the regression model.

Training the nonparametric regression model

Six predictors were involved in the RF algorithm: EVI, elevation, slope, aspect, latitude, and longitude (Ranhao et al 2008). All the predictor data sets had been resampled to

0.25 × 0.25° resolution by pixel averaging and reprojected onto the identical projection of the TRMM. The new data sets were separated into a training set and a test set. The training data were fed into the RF algorithm to establish a nonparametric regression model based on relationships between precipitation and environmental predictors. We employed a measure called mean decrease in accuracy (Equation 1) (Liaw and Wiener 2002; Cutler et al 2012) by using the R package "randomForest" to rank predictor importance. The test set was used to evaluate the model performance at coarse resolution.

Downscaling TRMM 3B43 annual precipitation data

The nonparametric regression model built in the previous step was used in the downscaling of TRMM 3B43 annual precipitation data. The downscaling method used in this study was developed on the basis of earlier studies (Immerzeel et al 2009; Jia et al 2011; Duan and Bastiaanssen 2013; Park 2013), in which TRMM 3B43 precipitation values were decomposed into deterministic trends and stochastic residuals. The downscaling procedure was as follows:

- Annual precipitation at 0.25° was predicted for 2001–2012 using the nonparametric regression model.
- The residual values for 2001–2012 were computed by subtracting the predicted annual precipitation from the original TRMM annual precipitation data.
- Because the residual data are regularly spaced and the spline interpolator is typically used for this kind of data (Immerzeel et al 2009; Duan and Bastiaanssen 2013), and the tests showed that the simple spline tension interpolator generated a smoother map than other methods (such as kriging and inverse distance weighting), the residual maps were interpolated into a resolution of 1 km using bilinear interpolation.
- The annual downscaled precipitation values at 1-km resolution for 2001–2012 were estimated from EVI, altitude, slope, latitude, and longitude at 1-km resolution using the nonparametric regression models trained for every year.
- Downscaled precipitation products were corrected by adding the residual values.

Calibrating downscaled precipitation data

The additive calibration method developed by Condom et al (2011) and Duan and Bastiaanssen (2013) was used to calibrate downscaled precipitation values to minimize the difference between them and measured precipitation from rain gauges. The calibration procedure was as follows:

- The differences between the downscaled precipitation values and the precipitation measures from rain gauge stations were computed.

- The point-based difference values were interpolated into a resolution of 1 km using latitude, longitude, and elevation of the rain gauges with a simple kriging interpolation technique, which is typically used with data of this type. Testing also showed that simple kriging outperformed other interpolation methods, such as spline and inverse distance weighting.
- Precipitation values downscaled at 1-km resolution were corrected to obtain the final calibrated precipitation by adding the above difference values.

Disaggregating annual precipitation data into monthly data

Duan and Bastiaanssen (2013) developed a simple fraction method derived from original TRMM 3B43 monthly data to downscale TRMM 3B43 data at monthly scales. The 1-km annual downscaled precipitation was finally disaggregated into 1-km monthly precipitation values using this fraction function. The procedure was as follows:

- The monthly fractions, which were used to disaggregate the annual precipitation, were defined as

$$Fraction_{i,j} = \frac{TRMM_{original,\,i,j}}{\sum_{i=1}^{n} TRMM_{original,\,i,j}} \tag{2}$$

where $TRMM_{original,i,j}$ is the precipitation that occurs during the ith month (n = 12) of the jth year (j = 2001, 2002, …, 2012) as estimated from the original TRMM 3B43 data.

- Because the fractions are regularly spaced like residual values, the fractions map of 0.25° resolution was interpolated into a spatial resolution of 1 km using a simple spline tension interpolator.
- The annual downscaled precipitation values at 1-km resolution were disaggregated into monthly downscaled precipitation values by multiplying the fraction values.
- The downscaled monthly precipitation values were calibrated with rain gauge data using an additive calibration method similar to that described above.

Validation

The accuracy of the downscaled products at annual and monthly scales was validated against the in situ measures from the rain gauge stations that were not used for calibration. Here, we calculated the coefficient determination (R^2), the root mean square error (RMSE), the mean absolute error (MAE), and the bias. They were defined as follows (Equations 3, 4, 5, and 6):

$$R^2 = \left(\frac{\sum_{i=1}^{n} (O_i - \bar{O}) \sum_{i=1}^{n} (P_i - \bar{P})}{\sqrt{\sum_{i=1}^{n} (O_i - \bar{O})} \sqrt{\sum_{i=1}^{n} (P_i - \bar{P})}} \right)^2 \qquad (3)$$

$$\text{RMSE} = \sqrt{\sum_{i=1}^{n} \frac{(O_i - P_i)^2}{n}} \qquad (4)$$

$$\text{MAE} = \frac{\sum_{i=1}^{n} |O_i - P_i|}{n} \qquad (5)$$

$$\text{Bias} = \frac{\sum_{i=1}^{n} P_i}{\sum_{i=1}^{n} O_i} - 1 \qquad (6)$$

where P_i is the value of the original TRMM 3B43 data, downscaled precipitation values, or final calibrated precipitation values extracted at the location of the ith rain gauge, O_i is the observed precipitation from the ith rain gauge, n is the total number of rain gauge stations used for validation, $\bar{P}$ is the average value of the estimated precipitation, and $\bar{O}$ is the average observed value.

Results and discussion

Annual results and discussion

We evaluated the model's performance in different climatic conditions by testing the downscaling and calibration procedure for 4 randomly chosen years: 2 wet years (2008 and 2012) and 2 dry years (2002 and 2006). Figure 3 shows the agreement between the annual TRMM 3B43 precipitation values and values produced by the regression model at a spatial resolution of 0.25°. All models for the 4 years passed the significance test ($R^2 = 0.98$ and $P < 0.0001$), and slight underestimations were found where the annual TRMM precipitation values were 419 mm/y for the 4 years. However, NDVI values tend to reach saturation (Martiny et al 2006) when the annual precipitation is above 1200 mm/y. A good correlation between rainfall and geospatial variables (NDVI and DEM) has been found for semiarid and arid areas ($R^2 = 0.79$–0.85) (Jia et al 2011; Duan and Bastiaanssen 2013). The initial testing analysis in this study also showed that the EVI-based model outperformed the NDVI-based model, especially for areas with more rainfall. A possible reason for this is that the EVI exhibits less saturated signals for high biomass conditions in humid areas. Our approach gives the best agreement between observed and predicted precipitation over a large area extending from arid to humid conditions.

We derived the annual precipitation at 1-km resolution with the downscaling–calibration procedure using NDVI, EVI, and 6 other predictors (Figure 4; see also *Supplemental data*, Figure S1; http://dx.doi.org/10.1659/MRD-JOURNAL-D-14-00119.S1). In the results, hotspots (regions that

receive more precipitation than their surroundings) shown in the original TRMM precipitation map were better preserved in the downscaled map inferred with the EVI-based method than in the map based on the NDVI-based method. A number of similarities in spatial distribution in the estimated precipitation data can be seen in *Supplemental data*, Figure S2 (http://dx.doi.org/10.1659/MRD-JOURNAL-D-14-00119.S1). Less precipitation occurs in the western part of the Tibetan Plateau (annual precipitation is approximately 800–1000 mm); precipitation generally increases from northwest to southeast. The annual precipitation values show precipitation maxima of more than 2000 mm in the southern part of the plateau during the period covered by the study, even in dry years. Furthermore, more annual precipitation could be observed in the southwestern and eastern part of the plateau.

Original annual TRMM data and downscaled data without calibration obviously overestimated precipitation compared with rain gauge data. This result is consistent with previous research by Duan and Bastiaanssen (2013). Downscaled precipitation data with calibration achieved better agreement with rain gauge data than downscaled data without calibration for all years. The statistical indicators of the original, downscaled, and calibrated TRMM 3B43 precipitation data, validated against data from the rain gauge stations set aside for independent validation, are shown in Table 1.

Table 1 also shows that comparing original TRMM 3B43 and ground-measured precipitation, the R^2 ranges from 0.45 to 0.73 with a mean of 0.7. The original TRMM product shows a large bias value (around 0.2). The RMSE ranges from 135.17 to 287.50 mm, and the MAE ranges from 102.28 to 178.39 mm. The downscaling methods improved the accuracy with increased R^2 and reduced RMSE, MAE, and bias values for all 12 years, and considerable improvement could be observed in the wet years. This indicates that the downscaling procedure is indeed a step toward greater accuracy in assessing coarse-resolution precipitation data (Duan and Bastiaanssen 2013). However, the downscaled approach without calibration removes little of the bias in the estimates; the bias ranged from 0.3 to 0.1.

Table 1 also indicates that the calibrated downscaled method significantly improved results for the dry years: the average fitting R^2 was improved from 0.74 to 0.77 after calibration was applied to the original TRMM. For the wet years, the average R^2 was improved from approximately 0.70 to 0.76. Furthermore, the maximum RMSE for all years decreased from 252.69 mm to 215.10 mm and MAE from 169.62 mm to 144.54 mm. An average bias of 0.07 for all the years was achieved, whereas the original TRMM product had lower accuracy, with an average bias of 0.21 and downscaled precipitation with an average bias of 0.19. This suggests that the downscaling and calibration procedure does correct the bias between

FIGURE 3   Comparison of annual precipitation data from TRMM 3B43 and estimates based on random forest regression models.
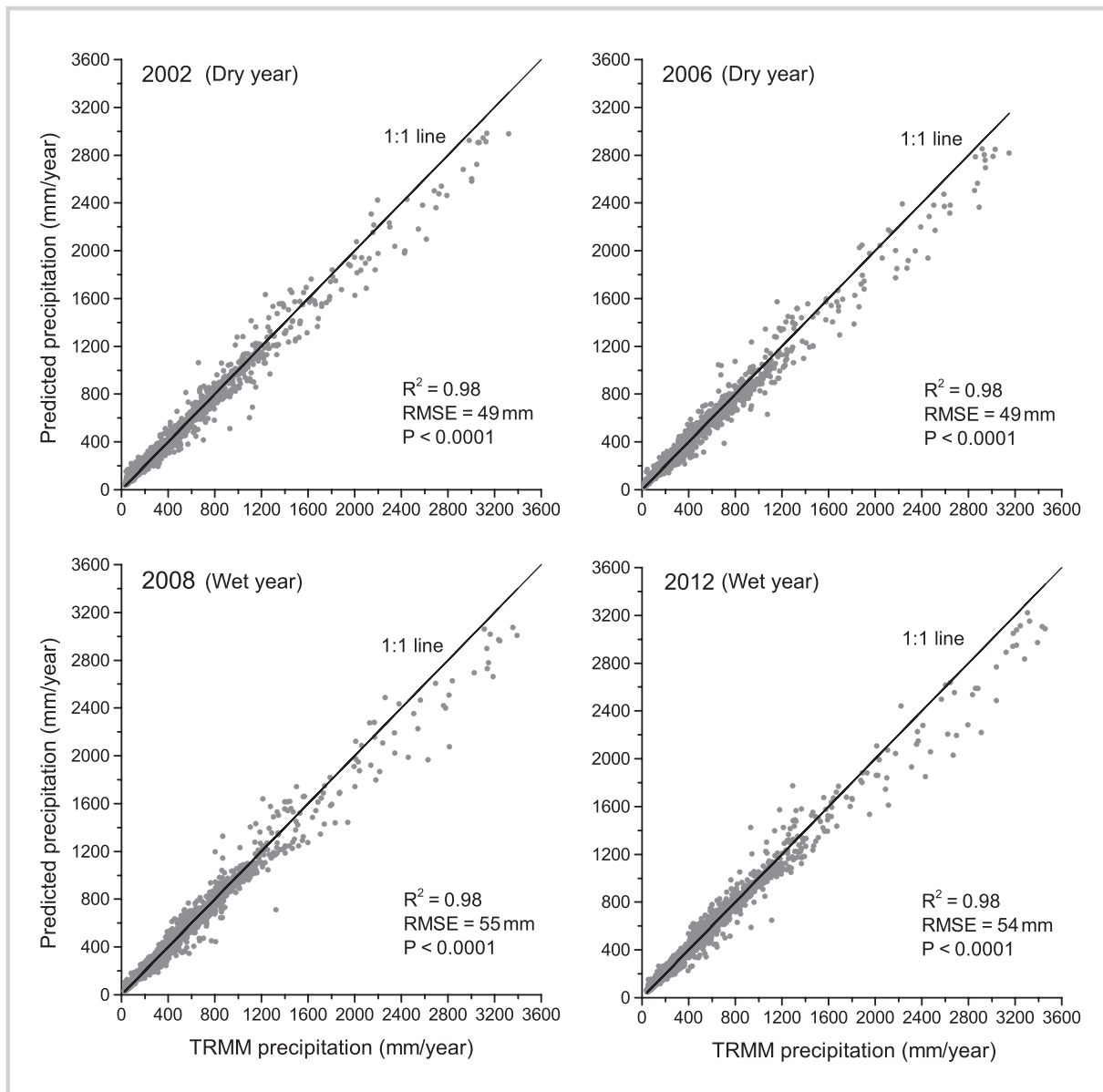
TRMM rainfall amount and measured quantities at gauge stations. It should be noted that only a few rain gauge stations exist in the western part of the Tibetan Plateau, and this inevitably limits the efficacy of the calibration method and the accuracy of the final rainfall data sets for this part of the plateau.

The importance of input predictors for the RF model is illustrated in Figure 5, which shows that the EVI, latitude, longitude, and elevation are key elements for statistical downscaling. For the whole study area, latitude contributes more to the model simulation than the other predictors.

Monthly results and discussion

The annual downscaled precipitation values with RF regression were disaggregated into 1-km monthly data using the fraction function (Equation 2). We randomly split monthly rain gauge data into 2 sample sets. The first set was used to calibrate the monthly disaggregated precipitation data using the additive calibration method. The second set was used as an independent validation set to test the method's performance by testing the downscaling and calibration procedure for the same randomly chosen years (2008 and 2012 for wet years and 2002 and 2006 for dry years). We compared monthly data

TABLE 1 Original (O), downscaled (D), and final calibrated (C) TRMM 3B43 precipitation data validated against data from independent rain gauge stations on the Tibetan Plateau for 2001–2012[a)] (Table 1 extended on next page).

	Wet years				Dry years	
	2001	2002	2006	2009	2003	2004
Mean_C	591.63	552.12	459.31	646.92	505.03	452.94
Mean_D	625.54	621.93	491.67	672.18	590.23	490.16
Mean_O	634.13	631.05	503.76	574.80	588.08	675.31
R^2_C	0.80	0.77	0.79	0.71	0.59	0.78
R^2_D	0.76	0.76	0.77	0.66	0.48	0.77
R^2_O	0.73	0.65	0.76	0.33	0.63	0.45
RMSE_C	215.10	152.89	98.63	205.01	152.67	98.94
RMSE_D	252.69	182.00	116.41	235.65	208.76	116.69
RMSE_O	263.65	218.66	135.17	280.71	205.49	287.50
MAE_C	144.54	113.74	69.93	134.99	117.71	69.71
MAE_D	169.62	117.91	86.72	151.71	149.59	85.14
MAE_O	178.39	127.10	102.28	163.48	132.53	177.64
Bias_C	0.22	0.00	0.02	0.20	0.04	0.04
Bias_D	0.29	0.13	0.13	0.25	0.22	0.13
Bias_O	0.31	0.14	0.16	0.32	0.14	0.25

FIGURE 4 Comparison of precipitation estimates derived with EVI- and NDVI-based methods. Original annual precipitation data from TRMM 3B43 are at 0.25° resolution for 2006; other products are at 1-km resolution. The circles in the TRMM 3B43 map denote regions that receive more precipitation than their surroundings.
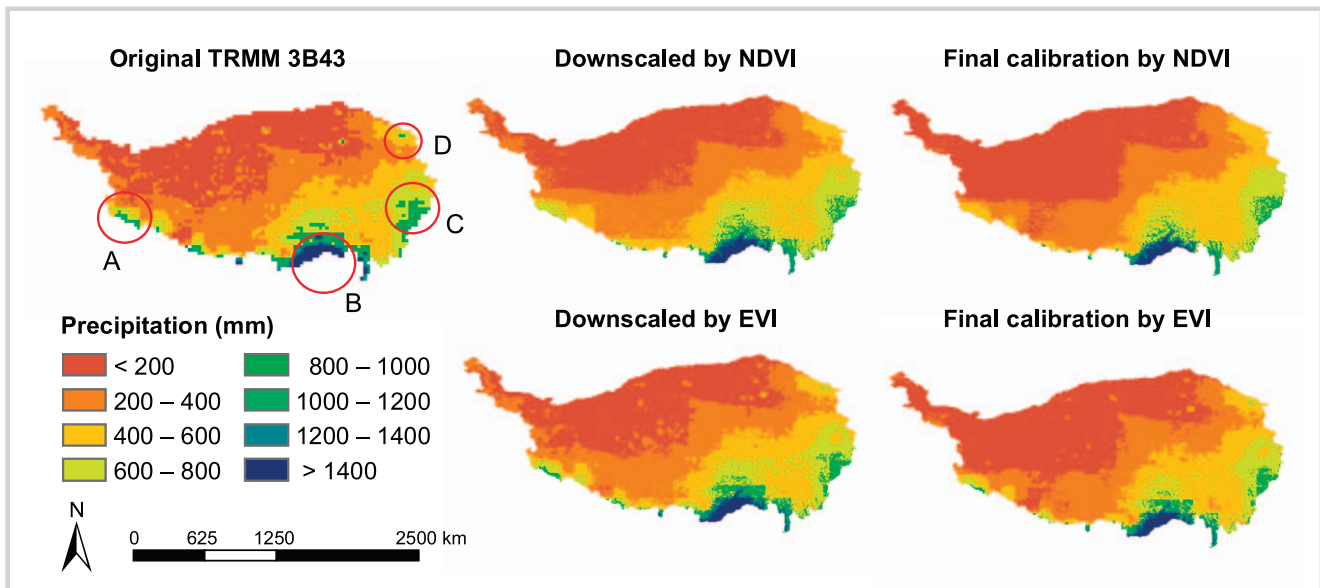
TABLE 1 (extended) Original (O), downscaled (D), and final calibrated (C) TRMM 3B43 precipitation data validated against data from independent rain gauge stations on the Tibetan Plateau for 2001–2012[a] (Table 1 began on previous page).

	Dry years					
	2005	2007	2008	2010	2011	2012
Mean_C	539.26	512.31	516.78	545.84	462.22	535.17
Mean_D	581.51	555.04	557.81	621.53	567.45	626.45
Mean_O	577.19	571.40	559.69	616.33	577.49	639.63
R^2_C	0.77	0.85	0.85	0.71	0.70	0.69
R^2_D	0.76	0.82	0.82	0.57	0.53	0.61
R^2_O	0.51	0.68	0.71	0.51	0.51	0.49
RMSE_C	157.60	127.27	127.86	145.32	122.30	181.87
RMSE_D	179.40	160.59	162.32	219.04	177.97	230.64
RMSE_O	204.98	190.81	193.26	228.68	186.17	266.81
MAE_C	107.13	92.26	93.65	97.44	93.41	126.26
MAE_D	125.62	116.81	118.05	152.76	121.37	149.89
MAE_O	135.13	122.52	128.11	151.89	125.57	166.53
Bias_C	0.11	0.09	0.03	0.10	−0.05	0.02
Bias_D	0.20	0.18	0.18	0.25	0.16	0.20
Bias_O	0.19	0.18	0.19	0.24	0.19	0.22

[a] R, correlation coefficient; RMSE, root-mean-square error; MAE, mean absolute error.

from the rain gauges with the corresponding values from the original TRMM 3B43 and downscaled and calibrated values (Figure 6). Downscaled and calibrated monthly values were in good agreement with measured rain gauge data (R^2 = 0.78, RMSE = 24.59 mm, MAE = 13.61 mm, bias = 0.01). Similar results were also observed for downscaled monthly values without calibration (R^2 = 0.78, RMSE = 24.65 mm, MAE = 13.81 mm, bias = 0.04). Downscaling alone already improved accuracy with increased R^2 and reduced RMSE, MAE, and bias values, compared with original monthly TRMM 3B43 data (R^2 = 0.73, RMSE = 31 mm, MAE = 16 mm, bias = 0.17). The fraction-calibrated downscaling method dramatically improved the average bias value from 0.17 to 0.01. That means it is valid to use this method to estimate monthly values for the complex plateau area.
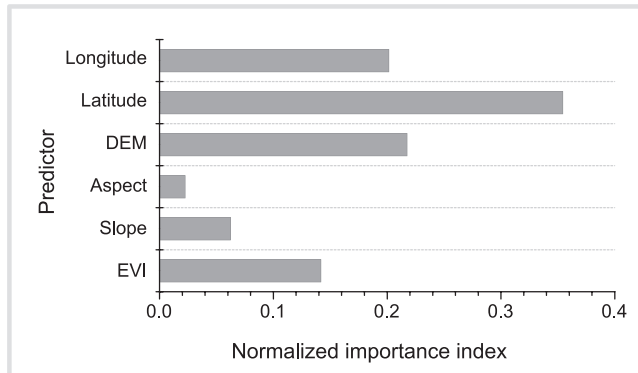
Figure 7 shows time series of the mean monthly precipitation, R^2, RMSE, MAE, and bias for the 4 randomly chosen years. To make comparisons among different months by considering monthly variations in rainfall, we computed the MAE (as a percentage of the mean value from corresponding rain gauge observations). Downscaled monthly precipitation data agreed well with measured monthly rain gauge data (Figure 7A). The R^2 for the growing season (February to June) and the season in which deciduous trees turn color and lose their leaves was higher than that for the other seasons (July to

January) (Figure 7B). The RMSE and bias values had almost the same variation pattern (Figure 7C–E). MAE values reached a peak in the dry season, whereas low values occurred in the wet season. This is consistent with findings by Duan and Bastiaanssen (2012) that their method made fewer errors in the wet season and more in the dry season. Calibrated downscaling significantly improved TRMM 3B43 data (Figure 7E). The winter months (December to February) showed more errors, with an average bias higher than 0.63, whereas bias values lower than 0.13 were often observed in other months. Figure 7E also suggests that the disaggregation method can reduce the MAE and bias for almost all seasons, though overall the improvement is not remarkable.

Conclusions

In this study, we developed a nonparametric downscaling method to qualify the spatial distribution of precipitation on the Tibetan Plateau, an area for which ground observations are lacking. We tested the performance of the nonparametric statistical model and found that it gives the best agreement between original and predicted TRMM precipitation (all R^2 = 0.98). An additive calibration procedure was carried out to remove the discrepancy between the point measurement and

FIGURE 5 Importance of geospatial predictors for precipitation downscaling illustrated by the mean decrease in accuracy of attributes as assigned by the RF.

FIGURE 6 Comparison of monthly precipitation measured by rain gauge stations with (A) original TRMM 3B43 data; (B) downscaled data; (C) calibrated data.

downscaled precipitation estimation. We found the disaggregation procedure with calibration, which was used to produce monthly precipitation, can reduce the MAE and bias for almost all seasons but did not greatly improve the overall accuracy of precipitation estimates at the monthly scale. The final annual and monthly rainfall data at 1-km resolution over the Tibetan Plateau for 2001 to 2012 were obtained using the integrated downscaling–calibration method.

Because the study covered an area, the Tibetan Plateau, with a variety of climate conditions and complex topography, the technique it tested is likely to also be effective elsewhere in the world. However, a number of important limitations need to be considered.

First, although most of the precipitation occurs in the rainy season, snow is the main form of precipitation in some Tibetan Plateau regions. This can affect the accuracy of the precipitation data, and thus affect the efficiency of the algorithm, in the following ways:

- The presence of snow and/or ice greatly changes the reflectance of the land surface and contaminates the vegetation index (Shen 2011).
- As indicated by its name, TRMM was primarily designed to measure tropical rainfall. Snow and ice on the ground scatter microwave energy in a similar fashion to ice crystals and raindrops in the atmosphere, so the precipitation estimates may perform poorly during the winter (Yin et al 2008).
- The final precipitation data are not robust because rain gauges can be disturbed by wind and blocked by snow or ice (Adam and Lettenmaier 2003).

Secondly, this study did not investigate the application of downscaling techniques to water bodies and urban areas, though the method gives fine precipitation estimates in those areas. Precipitation over water bodies can be derived because the method in essence is an ensemble decision-tree model with several geospatial predictors. Even if the EVI value is very low or negative, the method still can generate precipitation data for those
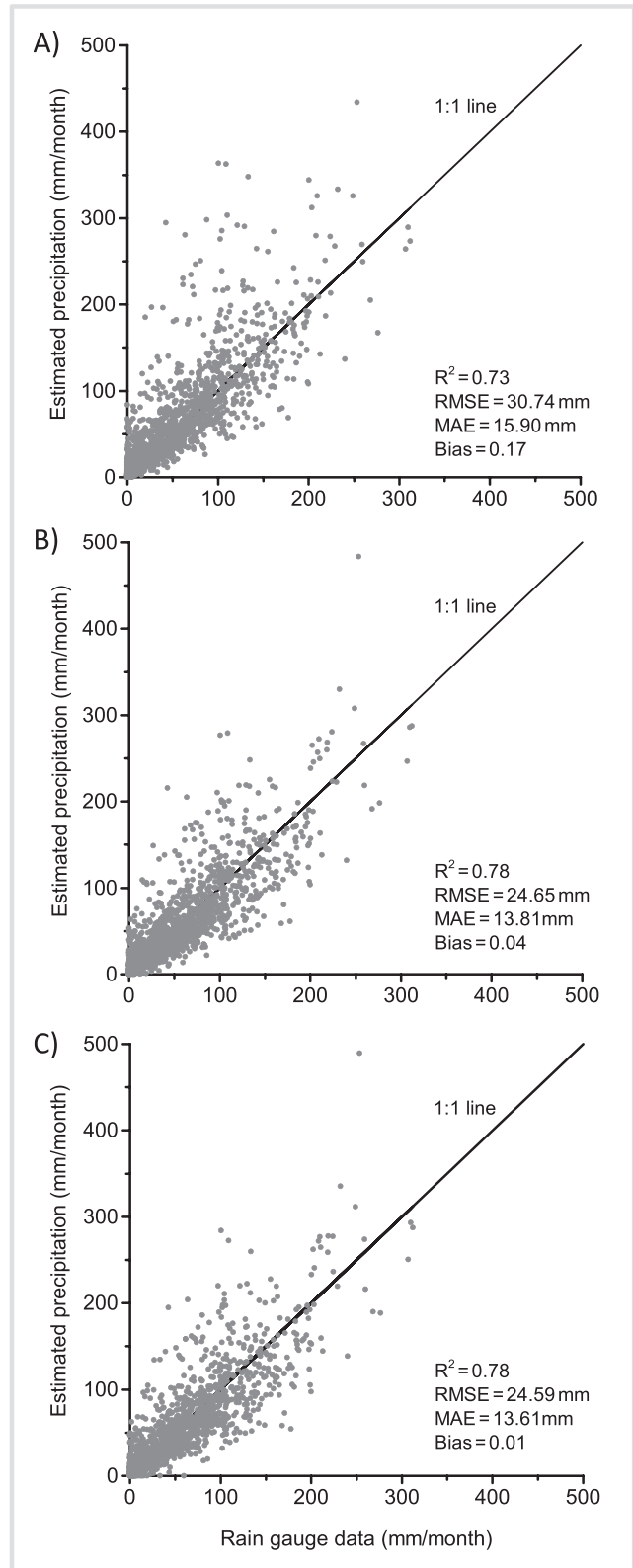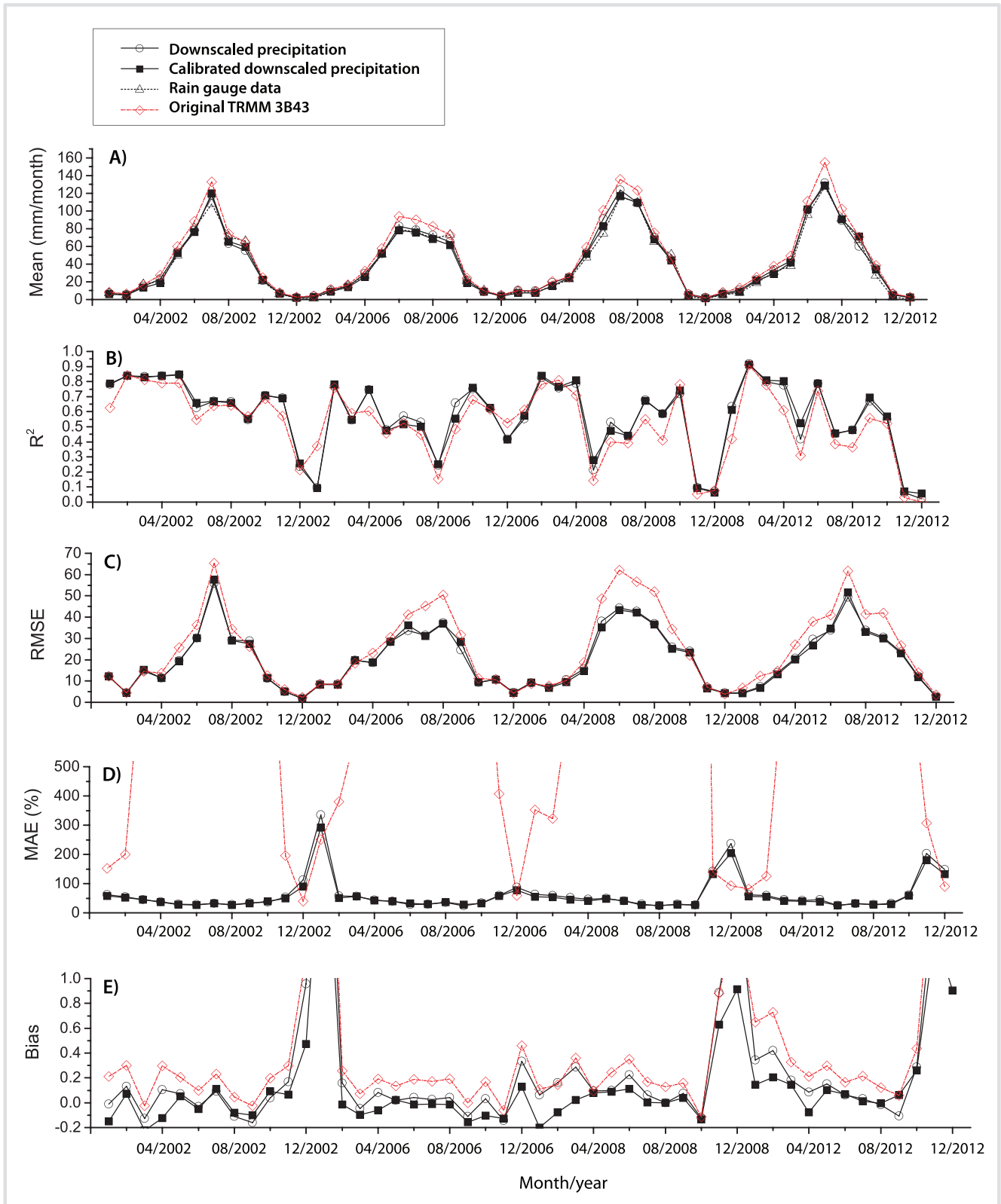
FIGURE 7 Time series for statistics for 2002, 2006, 2008, and 2012 for all stations used in validation: A) mean monthly precipitation; B) R2; C) RMSE; D) MAE; E) bias.

areas. However, the accuracy of the precipitation estimates over water bodies could not be assessed because there are no rain gauges there.

Finally, we cannot completely explain the variability and interaction of geospatial factors and the precipitation dynamic, and some of the predictors may not well explain the variance of the estimates. And most of the rain gauge

stations used in this study are in the south and east part of the Tibetan Plateau, which may affect the performance of GDA calibration. A natural progression of this work would be to account for bias correction of snowfall measurement and geophysical mechanisms of precipitation, and assess the performance and utility of these techniques in other parts of the world.

REFERENCES

Adam JC, Lettenmaier DP. 2003. Adjustment of global gridded precipitation for systematic bias. *Journal of Geophysical Research: Atmospheres* 108(D9): 4257.

Agam N, Kustas WP, Anderson MC, Li F, Neale CMU. 2007. A vegetation index based technique for spatial sharpening of thermal imagery. *Remote Sensing of Environment* 107(4):545–558.

Almazroui M. 2011. Calibration of TRMM rainfall climatology over Saudi Arabia during 1998–2009. *Atmospheric Research* 99(3):400–414.

Breiman L. 2001. Random forests. *Machine Learning* 45(1):5–32.

Chan JCW, Paelinckx D. 2008. Evaluation of Random Forest and Adaboost tree-based ensemble classification and spectral band selection for ecotope mapping using airborne hyperspectral imagery. *Remote Sensing of Environment* 112(2):2999–3011.

Che M, Chen B, Innes JL, Wang G, Dou X, Zhou T, Zhang H, Yan J, Xu G, Zhao H. 2014. Spatial and temporal variations in the end date of the vegetation growing season throughout the Qinghai–Tibetan Plateau from 1982 to 2011. *Agricultural and Forest Meteorology* 189:81–90.

Cheema MJM, Bastiaanssen WGM. 2012. Local calibration of remotely sensed rainfall from the TRMM satellite for different periods and spatial scales in the Indus Basin. *International Journal of Remote Sensing* 33(8): 2603–2627.

Chen F, Liu Y, Liu Q, Li X. 2014. Spatial downscaling of TRMM 3B43 precipitation considering spatial heterogeneity. *International Journal of Remote Sensing* 35(9):3074–3093.

Condom T, Rau P, Espinoza JC. 2011. Correction of TRMM 3B43 monthly precipitation data over the mountainous areas of Peru during the period 1998–2007. *Hydrological Processes* 25:1924–1933.

Cutler A, Cutler DR, Stevens JR. 2012. Random forests. *In:* Zhang C, Yunqian M, editors. *Ensemble Machine Learning: Methods and Applications.* New York, NY: Springer Science+Business Media, pp 157–175.

Duan Z, Bastiaanssen WGM. 2013. First results from Version 7 TRMM 3B43 precipitation product in combination with a new downscaling-calibration procedure. *Remote Sensing of Environment* 131:1–13.

Gessner U, Naeimi V, Klein I, Kuenzer C, Klein D, Dech S. 2013. The relationship between precipitation anomalies and satellite-derived vegetation activity in Central Asia. *Global and Planetary Change* 110:74–87.

Giannoni F, Smith JA, Zhang Y, Roth G. 2003. Hydrologic modeling of extreme floods using radar rainfall estimates. *Advances in Water Resources* 26:195–203.

Goovaerts P. 2000. Geostatistical approaches for incorporating elevation into the spatial interpolation of rainfall. *Journal of Hydrology* 228:113–129.

Guo J, Liang X, Leung LR. 2004. Impacts of different precipitation data sources on water budgets. *Journal of Hydrology* 298:311–334.

Heidinger H, Yarlequé C, Posadas A, Quiroz R. 2012. TRMM rainfall correction over the Andean Plateau using wavelet multi-resolution analysis. *International Journal of Remote Sensing* 33(14):4583–4602.

Huete A, Didan K, Miura T, Rodriguez EP, Gao X, Ferreira LG. 2002. Overview of the radiometric and biophysical performance of the MODIS vegetation indices. *Remote Sensing of Environment* 83:195–213.

Huffman GJ, Adler RF, Arkin P, Chang A, Ferraro R, Gruber A, Janowiak J, McNab A, Rudolf B, Schneider U. 1997. The Global Precipitation Climatology Project (GPCP) combined precipitation dataset. *Bulletin of the American Meteorological Society* 78:5–20.

Huffman GJ, Bolvin DT. 2013. *TRMM and Other Data Precipitation Data Set Documentation.* Greenbelt, MD: Laboratory for Atmospheres, NASA Goddard Space Flight Center and Science Systems and Applications. ftp://precip.gsfc. nasa.gov/pub/trmmdocs/3B42_3B43_doc.pdf; accessed on 17 March 2015.

Huffman GJ, Bolvin DT, Nelkin EJ, Wolff DB, Adler RF, Gu G, Hong Y, Bowman KP, Stocker EF. 2007. The TRMM Multisatellite Precipitation Analysis (TMPA): Quasi-global, multiyear, combined-sensor precipitation estimates at fine scales. *Journal of Hydrometeorology* 8:38–55.

Hughes DA, Smakhtin V. 1996. Daily flow time series patching or extension: A spatial interpolation approach based on flow duration curves. *Hydrological Sciences Journal* 41:851–871.

Hunink JE, Immerzeel WW, Droogers P. 2014. A high-resolution precipitation 2-step mapping procedure (HiP2P): Development and application to a tropical mountainous area. *Remote Sensing of Environment* 140:179–188.

Ibarra-Berastegi G, Saénz J, Ezcurra A, Elías A, Argandoña JD, Errasti I. 2011. Downscaling of surface moisture flux and precipitation in the Ebro Valley (Spain) using analogues and analogues followed by random forests and multiple linear regression. *Hydrology and Earth System Sciences* 15:1895–1907.

Immerzeel WW, Quiroz RA, de Jong SM. 2005. Understanding precipitation patterns and land use interaction in Tibet using harmonic analysis of SPOT VGT-S10 NDVI time series. *International Journal of Remote Sensing* 26:2281–2296.

Immerzeel WW, Rutten MM, Droogers P. 2009. Spatial downscaling of TRMM precipitation using vegetative response on the Iberian Peninsula. *Remote Sensing of Environment* 113:362–370.

Jia S, Zhu W, Lü A, Yan T. 2011. A statistical spatial downscaling algorithm of TRMM precipitation based on NDVI and DEM in the Qaidam Basin of China. *Remote Sensing of Environment* 115:3069–3079.

Justice CO, Vermote E, Townshend JRG, Defries R, Roy DP, Hall DK, Salomonson VV, Privette JL, Riggs G, Strahler A, Lucht W, Myneni RB, Knyazikhin Y, Running SW, Nemani RR, et al. 1998. The Moderate Resolution Imaging Spectroradiometer (MODIS): Land remote sensing for global change research. *IEEE Transactions on Geoscience and Remote Sensing* 36:1228–1249.

Kubota T, Shige S, Hashizume H, Aonashi K, Takahashi N, Seto S, Hirose M, Takayabu YN, Ushio T, Nakagawa K, Iwanami K. 2007. Global precipitation map using satellite-borne microwave radiometers by the GSMaP project: Production and validation. *IEEE Transactions on Geoscience and Remote Sensing* 45:2259–2275.

Kummerow C, Simpson J, Thiele O, Barnes W, Chang ATC, Stocker E, Adler RF, Hou A, Kakar R, Wentz F, Ashcroft P, Kozu T, Hong Y, Okamoto K, Iguchi T, et al. 2000. The status of the Tropical Rainfall Measuring Mission (TRMM) after two years in orbit. *Journal of Applied Meteorology* 39(12):1965–1982.

Kyriakidis PC, Kim J, Miller NL. 2001. Geostatistical mapping of precipitation from rain gauge data using atmospheric and terrain characteristics. *Journal of Applied Meteorology* 40:1855–1877.

Langella G, Basile A, Bonfante A, Terribile F. 2010. High-resolution space-time rainfall analysis using integrated ANN inference systems. *Journal of Hydrology* 387:328–342.

Liaw A, Wiener M. 2002. Classification and regression by random forest. *R News* 2:18–22.

Martiny N, Camberlin P, Richard Y, Philippon N. 2006. Compared regimes of NDVI and rainfall in semi-arid regions of Africa. *International Journal of Remote Sensing* 27(23):5201–5223.

Maussion F, Scherer D, Mölg T, Collier E, Curio J, Finkelnburg R. 2014. Precipitation seasonality and variability over the Tibetan Plateau as resolved by the high Asia reanalysis. *Journal of Climate* 27(5):1910–1927.

Michaelides S, Levizzani V, Anagnostou E, Bauer P, Kasparis T, Lane JE. 2009. Precipitation: Measurement, remote sensing, climatology and modeling. *Atmospheric Research* 94:512–533.

Park N-W. 2013. Spatial downscaling of TRMM precipitation using geo-statistics and fine scale environmental variables. *Advances in Meteorology* 2013(11):1–9.

Piao S, Cui M, Chen A, Wang X, Ciais P, Liu J, Tang Y. 2011. Altitude and temperature dependence of change in the spring vegetation green-up date from 1982 to 2006 in the Qinghai-Xizang Plateau. *Agricultural and Forest Meteorology* 151(12):1599–1608.

Quiroz R, Yarlequé C, Posadas A, Mares V, Immerzeel WW. 2011. Improving daily rainfall estimation from NDVI using a wavelet transform. *Environmental Modelling & Software* 26:201–209.

Ran Y, Li X, Lu L. 2009. China land cover classification at 1 km spatial resolution based on a multi-source data fusion approach. *Advances in Earth Science* 24(2):192–203.

Ranhao S, Baiping Z, Jing T. 2008. A multivariate regression model for predicting precipitation in the Daqing Mountains. *Mountain Research and Development* 28:318–325.

Schuurmans JM, Bierkens MFP. 2007. Effect of spatial distribution of daily rainfall on interior catchment response of a distributed hydrological model. *Hydrology and Earth System Sciences Discussions* 11:677–693.

Shen M. 2011. Spring phenology was not consistently related to winter warming on the Tibetan Plateau. *Proceedings of the National Academy of Sciences of the United States of America* 108(19):E91–E92.

Shen M, Tang Y, Chen J, Zhu X, Zheng Y. 2011. Influences of temperature and precipitation before the growing season on spring phenology in grasslands of the central and eastern Qinghai-Tibetan Plateau. *Agricultural and Forest Meteorology* 151(12):1711–1722.

Stumpf A, Kerle N. 2011. Object-oriented mapping of landslides using random forests. *Remote Sensing of Environment* 115:2564–2577.

Vincenzi S, Zucchetta M, Franzoi P, Pellizzato M, Pranovi F, Leo GAD, Torricelli P. 2011. Application of a random forest algorithm to predict spatial distribution of the potential yield of *Ruditapes philippinarum* in the Venice Lagoon, Italy. *Ecological Modelling* 222:1471–1478.

Wei C-L, Rowe GT, Escobar-Briones E, Boetius A, Soltwedel T, Julian M, Soliman Y, Huettmann F, Qu F, Yu Z, Pitcher CR, Richard L, Wicksten MK, Rex MA, Baguley JG, et al. 2010. Global patterns and predictions of seafloor biomass using random forests. *PLoS One* 5:e15323.

Xia Z. 2014. *Mapping Mean Average Annual Precipitation Across China Mainland in the Period 2001–2010 From TRMM 3B43 Product Using Spatial Downscaling Approaches* [MSc thesis]. Nanjing, China: Nanjing University of Information Science and Technology.

Yin Z-Y, Zhang X, Liu X, Colella M, Chen X. 2008. An assessment of the biases of satellite rainfall estimates over the Tibetan Plateau and correction methods based on topographic analysis. *Journal of Hydrometeorology* 9(3): 301–326.

Yu X, Hyyppä J, Vastaranta M, Holopainen M, Viitala R. 2011. Predicting individual tree attributes from airborne laser point clouds based on the random forests technique. *ISPRS Journal of Photogrammetry and Remote Sensing* 66: 28–37.

Zhang Y-L, Li B-Y, Zheng D. 2002. A discussion on the boundary and area of the Tibetan Plateau in China. *Geographical Research* 21:1–8.

Zheng X, Zhu J. 2014. A methodological approach for spatial downscaling of TRMM precipitation data in North China. *International Journal of Remote Sensing* 36(1):144–169.

Zhisheng A, Kutzbach JE, Prell WL, Porter SC. 2001. Evolution of Asian monsoons and phased uplift of the Himalaya Tibetan plateau since Late Miocene times. *Nature* 411(6833):62–66.

Zhong L, Su Z, Ma Y, Salama MS, Sobrino JA. 2011. Accelerated changes of environmental conditions on the Tibetan Plateau caused by climate change. *Journal of Climate* 24(24):6540–6550.

Supplemental data

FIGURE S1 The range (mean $\pm$ standard deviation) of R^2 and RMSE for predictions using the EVI- and NDVI-based methods. Annual precipitation (A) > 0 mm/y; (B) > 1000 mm/y; (C) > 2000 mm/y.

FIGURE S2 Annual precipitation on the Tibetan Plateau at spatial resolution 1×1 km for 2001–2012, aggregated from the final calibrated TRMM 3B43 precipitation.

Found at DOI: 10.1659/MRD-JOURNAL-D-14-00119.S1 (176 KB PDF).